Journal of Alloys and Compounds 506 (2010) 820–825

Contents lists available at ScienceDirect

Journal of Alloys and Compounds

journal homepage: www.elsevier.com/locate/jallcom

Discussing the precipitation behavior of σ phase using diffusion equation and thermodynamic simulation in dissimilar stainless steels

Chih-Chun Hsieh, Weite Wu*

Department of Materials Science and Engineering, National Chung Hsing University, 250 Kuo-Kuang Rd., Taichung 402, Taiwan

ARTICLE INFO

Article history:
Received 25 February 2010
Received in revised form 7 July 2010
Accepted 10 July 2010
Available online 17 July 2010

Keywords:
Intermetallics
Precipitation
Diffusion
Microstructure
Phase transitions
Metallography

ABSTRACT

This study performed a precipitation examination of the σ phase using the Vitek diffusion equation and thermodynamic simulation in dissimilar stainless steels during multi-pass welding. The results of the experiment demonstrate that the diffusion rates (D^{δ}_{Cr} and D^{δ}_{Ni}) of Cr and Ni are higher in δ-ferrite than (D^{γ}_{Cr} and D^{γ}_{Ni}) in the γ phase and that they facilitate the precipitation of σ phase in the third pass fusion zone. When the diffusion activation energy of Cr in δ-ferrite is equal to that of Ni in δ-ferrite ($Q^{\delta}_{d\,Cr} \fallingdotseq Q^{\delta}_{d\,Ni}$), phase transformation of the $\delta \rightarrow \sigma$ can be occurred.

1. Introduction

Austenitic and ferritic stainless steel composites possessing low carbon content are used extensively in high temperature applications such as energy conversion systems. For instance, to ensure economy in central power stations, sections of boilers subjected to lower temperatures are constructed from ferritic stainless steel for economic reasons [1].

When stainless steels are exposed to temperatures between 973 K and 1273 K for sustained periods of time, several undesirable intermetallic phases, such as σ, χ, and π, can precipitate [2–5]. The σ phase is the most serious of these secondary phases due to its impact on the mechanical properties, corrosion resistance or weldability of stainless steels, among other properties [6–9]. It has been demonstrated that the addition of alloying elements, Cr and Mo in particular, can accelerate the precipitation of σ phase at high temperatures [10]. This also enlarges the precipitation area in the time-temperature transformation (TTT) diagram, as reported by Atamert and King [11].

While the σ phase was first observed in the Fe–Cr system, it has also been observed in Fe–V, Fe–Mo, and Cr–Mo–Ni alloy systems [12]. The crystallographic lattice of the σ phase is a tetragonal structure with 30 atoms per unit cell. The σ phase has been found in more than 50 binary transition metal alloys and is of great interest for both scientific and technological purposes. Scientific interest is related to the gathering of knowledge regarding the physical properties of the phase, in particular those involved in the mechanism of its formation. Industrial interest originates from the fact that the σ phase often forms in materials that are technologically important, and its presence drastically deteriorates their properties [13].

Previous studies on the properties of stainless steel containing σ phase have concentrated on high temperature characteristics, considering embrittlement mechanisms, fracture toughness, and corrosion resistance [14] in the heat-affected zones (HAZ) of similar stainless steels. Very few works however, have addressed the high temperature properties in the fusion zones (FZ) of dissimilar stainless steels. The precipitation mechanism of σ phase in fusion zones during the welding process is unclear for austenitic and ferritic stainless steels.

This study uses autogenous welding to manufacture dissimilar stainless steels and discusses the precipitation behavior of σ phase in the fusion zone of dissimilar stainless steels taking place during the multi-pass GTAW (Gas Tungsten Arc Welding) process. This is done via a calculation of the Vitek diffusion equation. The objectives are to delineate the precipitation mechanism of the sigma phase in dissimilar stainless steels at various welding passes as well as to contribute to the understanding of the precipitation characteristics of the σ phase during the multi-pass GTAW process in dissimilar stainless steels.

* Corresponding author. Tel.: +886 4 22840500x604; fax: +886 4 22857017.
E-mail address: wwu@dragon.nchu.edu.tw (W. Wu).

0925-8388/$ – see front matter.
doi:10.1016/j.jallcom.2010.07.084

Table 1
Chemical composition of the raw samples.

Material	Element (wt.%)						
	Cr	Ni	Si	Mn	C	Mo	Fe
304 S.S.	19.2	10.9	1.0	2.0	0.08	1.22	Bal.
430 S.S.	18.3	–	0.75	1.0	0.12	1.18	Bal.

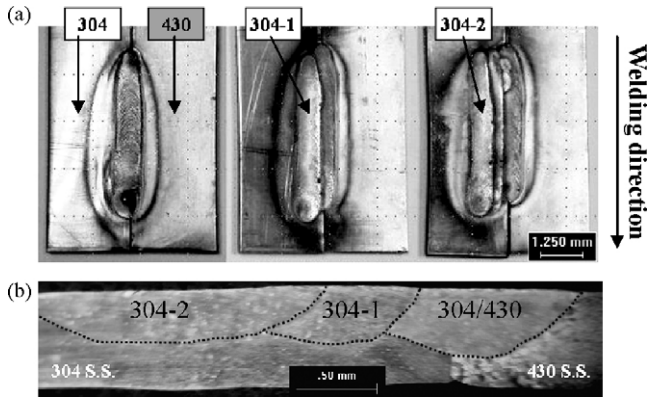

Fig. 1. Manufacturing process of the dissimilar stainless steels: (a) top view and (b) cross-section.

2. Experimental procedures

Two types of stainless steels, namely 304 and 430, were employed in the experiment. Both are representatives of fully austenite containing a small number of ferrite phases and fully ferritic microstructures, respectively. Their chemical compositions are listed in Table 1. The dimensions of the raw materials were 70 mm × 25 mm × 3 mm.

The composites of dissimilar stainless steels were created using an automatic GTAW process. The appearance of weld metal from dissimilar stainless steels is shown in Fig. 1. The multi-pass welding (304/430, 304-1, and 304-2) were preformed without filler at a welding current of 100 A and an arc voltage of 11 V with a travel speed of 120 mm/min. A series of symbols for 304/430, 304-1, and 304-2 were defined as the first, second, third pass welding, respectively. After the multi-pass welding, the samples were cooled to room temperature in air and mounted by molding epoxy, then ground using SiC paper and polished with Al_2O_3 powder paste.

The mounted samples were etched using a color etching technique with Murakami (10 g $K_3Fe(CN)_6$ + 10 g KOH + 100 ml H_2O) for 60 s in order to observe the δ-ferrite, σ phase, and γ phases in the third pass fusion zone (304-2). An electron probe micro-analyzer (JXA-8900R JEOL, EPMA) was employed to observe the δ-ferrite, σ phase, and γ phase. Their chemical compositions were identified using a wavelength dispersive spectrometer (WDS).

The peak temperatures and the endothermic and exothermic peaks were examined suing differential scanning calorimeter (NETZSCH DSC 404 C) in order to discuss the precipitation of $\delta \rightarrow \sigma + \gamma_2$. The specimens were heated from 600 °C to 1300 °C with a heating rate of 20 °C/s. Subsequently, the diffusion parameters were calculated using the Vitek diffusion equation to explain the phase transformation of the $\delta \rightarrow \sigma$. These diffusion parameters included diffusivity (D) and activation energy (Q).

The computer simulation was performed using Thermo-Calc software (TCW Version 2.2). The FEDAT database was utilized to simulate the phase diagram in the sample of the third pass fusion zone during the $\delta \rightarrow \sigma$ phase transformation for the purpose of further proving a series of experimental results.

3. Results and discussion

3.1. Precipitation of σ phase in the third pass fusion zone

In order to observe the precipitation behavior of the σ phase in the third pass fusion zone of the 304 stainless steels that occurred during the dissimilar welding. A color metallographic technique using Murakami's reagent was used to distinguish between other precipitates. The Murakami etching solution is an effective etching technique for revealing primary (δ and γ phases) as well as secondary phases (σ and γ_2 phases) in austenitic stainless steels. In Fig. 2(a) and (b), δ, σ, and γ_2, phases were colored blue, red, and ivory, respectively. It was discovered that the σ phase precipitated at the inner δ-ferrite particles in agreement with previous reports [15,16]. The Cr contents in δ-ferrite were consumed by the σ phase forming at the δ-ferrite. Based on what has been described above, the phase transformation of $\delta \rightarrow \sigma + \gamma_2$ occurred in the fusion zone subsequent to the third pass welding.

3.2. EPMA mapping and WDS quantitative analysis of σ phase in fusion zone

Because diffusion of Cr and Ni elements has a significant effect on the properties of stainless steels, it can be used to predict the precipitation of δ-ferrite, σ phase, and γ-austenite. A mapping analysis was performed on Cr, while Ni was assessed by EPMA, in order to further elucidate the σ phase precipitation in the fusion zone of the third pass welding. A secondary electron image (SEI) and the Cr and Ni concentration profiles of the fusion zones are presented in Fig. 2(a)–(c). The results reveal that the σ phase has an enriched level of Cr while the other regions show a depleted Cr profile, as shown in Fig. 2(b). Regarding Ni mapping, the distributions of Ni were concentrated on the austenite matrix, as illustrated in Fig. 2(c). Based on these results, the σ phase displayed Cr-rich and Ni-depleted profiles. However, the other positions showed greater concentrations of Cr surrounding the σ phase was identified as δ-ferrite after the multi-pass GTAW process.

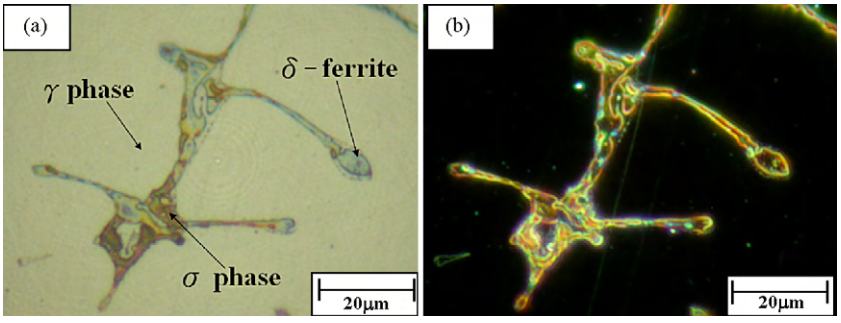

Fig. 2. Optical micrographs of δ-ferrite, σ phase, and γ phases in the third pass fusion zone during the $\delta \rightarrow \sigma$ phase transformation of: (a) bright field and (b) dark field.

Table 2
WDS analysis of precipitates in the fusion zone of the third pass welds.

Area	Element (wt.%)			
	Cr	Ni	Si	Fe
1 (σ)	35.74	4.24	5.85	55.72
2 (σ)	34.57	4.13	5.76	56.53
3 (σ)	35.32	4.45	5.82	57.44
4 (δ)	25.05	5.37	6.43	63.43
5 (γ)	18.76	8.34	3.34	65.48
6 (γ)	18.68	8.63	3.21	64.86

Elemental quantitative analyses with Fe, Cr, and Ni were performed utilizing a wavelength dispersive spectrometer (WDS) in order to verify the results of EPMA mapping. The results are presented in Table 2. The points #1–3 were identified as σ phase, because they showed the most enriched Cr levels among all regions. Nevertheless, point #4 displayed higher Cr and it determined as δ-ferrite. Furthermore, the δ and σ phases showed higher Si than γ-austenite. It was found that Si can enhance precipitation of δ and σ phases after the third pass welding. Lin et al. [17] also pointed out that Si is an efficient stabilizer for the δ-ferrite and σ phases, but accelerates their formation. Therefore, Si plays an important role of enhancing δ-ferrite transformation to σ phase. Furthermore, it presented a Ni-rich and Cr-depleted tendencies on points #5–6 and was identified as γ-austenite. In this research, the σ phase was a Fe–Cr–Si intermetallic compound, as described above.

Schematic diagrams explaining the mechanism of δ → σ in the fusion zone of third pass welding are shown in Fig. 3(a)–(d). Fig. 4(a)

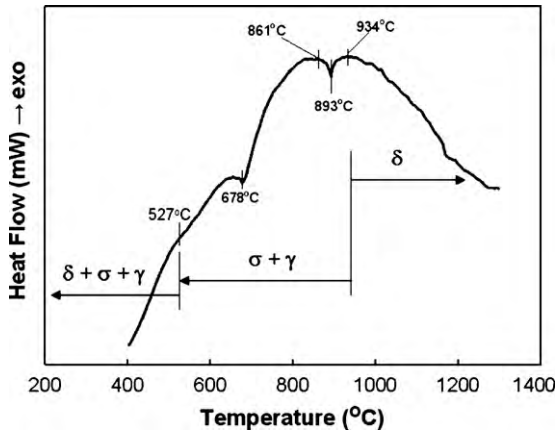

Fig. 5. DSC thermal analysis of the third pass fusion zone.

shows the initial state of δ → σ phase transformation. The Cr and Si elements then diffused from γ-austenite to δ-ferrite and σ phase subsequently formed at δ particles at the same time, as shown in Fig. 3(b). Moreover, Ni also diffused to the matrix from δ-ferrite and γ-austenite precipitation occurred when the σ phase formed, as indicated in Fig. 3(c).

3.3. Diffusion calculation

The formation of a σ phase includes temperature and elemental diffusion. Hence, this section will determine the precipitation

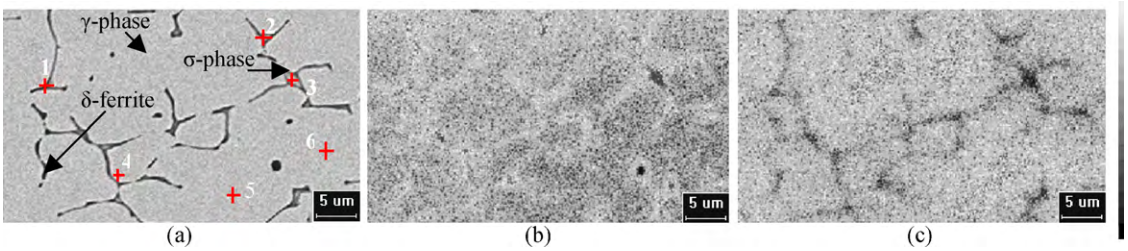

Fig. 3. The EPMA mapping analysis of σ phase after the third pass welding: (a) SEI micrograph, (b) Cr concentration profile and (c) Ni concentration profile.

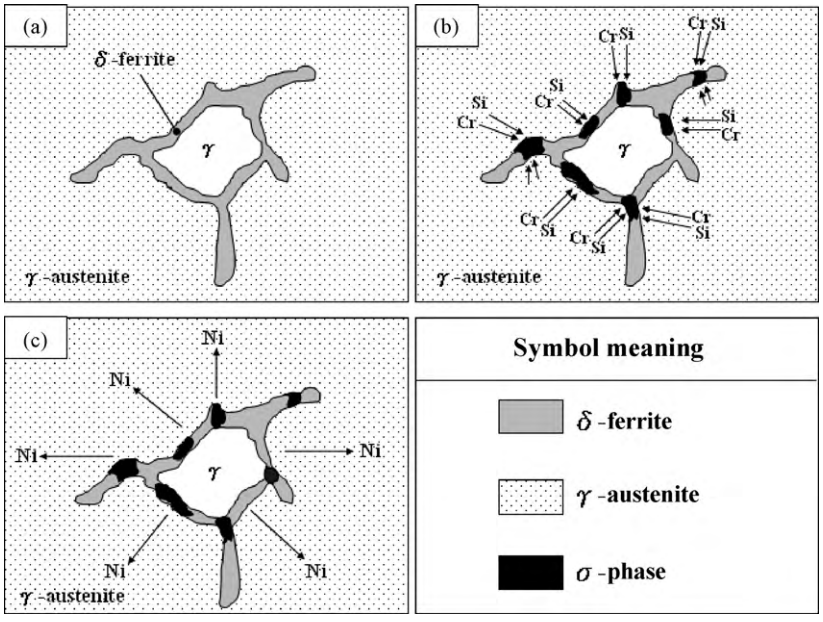

Fig. 4. Schematic showing the δ → σ phase transformation in the fusion zone of the third pass welds: (a) initial state, (b) σ phase formed at the inner δ particles and (c) Ni diffusion of δ and σ phases induced γ-austenite formation.

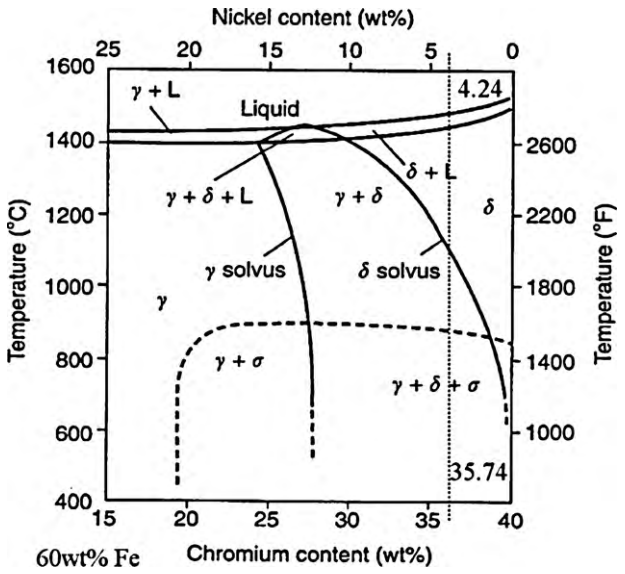

Fig. 6. The Fe–Cr–Ni phase diagram (60% Cr).

temperature of a σ phase using a differential scanning calorimeter (DSC) in an AISI 304 multi-pass welding system, as shown in Fig. 5. The diagram shows two exothermic and two endothermic peaks with peak temperatures of 861 °C, 934 °C, 678 °C, 893 °C, respectively. This is for the purpose of plotting the composition of the σ phase in this study (35 wt.% Cr, 4 wt.% Ni) to the Fe–Cr–Ni phase diagram shown in Fig. 6. Here, the solidification order was $L \rightarrow \delta + L \rightarrow \delta \rightarrow \delta + \gamma \rightarrow \gamma + \delta + \sigma$. The abovementioned results are marked out in Fig. 5. It was determined that the σ phase precipitates from 400 °C to 934 °C. Some researchers [18,19] have pointed out that the precipitation temperature of the σ phase is between 600 °C and 1000 °C. Specifically, the measured results of peak temperatures located within the precipitation temperature range of the σ phase were determined via DSC analysis. At these peak temperatures, the elemental diffusion behavior was significant on the $\delta \rightarrow \sigma$ phase transformation, e.g. Cr, Ni and Si during the multi-pass welding. This is due to the fact that these elements are beneficial for the formation of the δ and σ phases. Hsieh et al. [20] have reported that the Si can accelerate the $\delta \rightarrow \sigma$ at high elevated temperatures in stainless steels. It focuses on $\delta \rightarrow \sigma$ through the use of various diffusion theories drawing from DSC analysis results. Vitek et al. [21] pointed out that the diffusion of empirical equations on the study of the diffusion couple in stainless steels, labeled the "Vitek model", as illustrated in Eqs. (1)–(4). These formulas can be used to respectively calculate the diffusion coefficients of Cr and Ni in δ-ferrite and γ-austenite in most stainless steels:

$$D_{Cr}^{\delta} = 2 \exp\left(\frac{-28,866}{T}\right) \quad (1)$$

$$D_{Ni}^{\gamma} = 2.3 \exp\left(\frac{-35,722}{T}\right) \quad (2)$$

$$D_{Ni}^{\delta} = \left(\frac{D_{Cr}^{\delta}}{1.3}\right) \quad (3)$$

$$D_{Cr}^{\gamma} = 3.4 D_{Ni}^{\gamma} \quad (4)$$

The meanings of symbols for the Vitek Model are described as follows:

D_{Cr}^{δ} : Diffusion coefficient of Cr in δ-ferrite, $cm^2\ s^{-1}$

D_{Ni}^{γ} : Diffusion coefficient of Ni in γ-austenite, $cm^2\ s^{-1}$

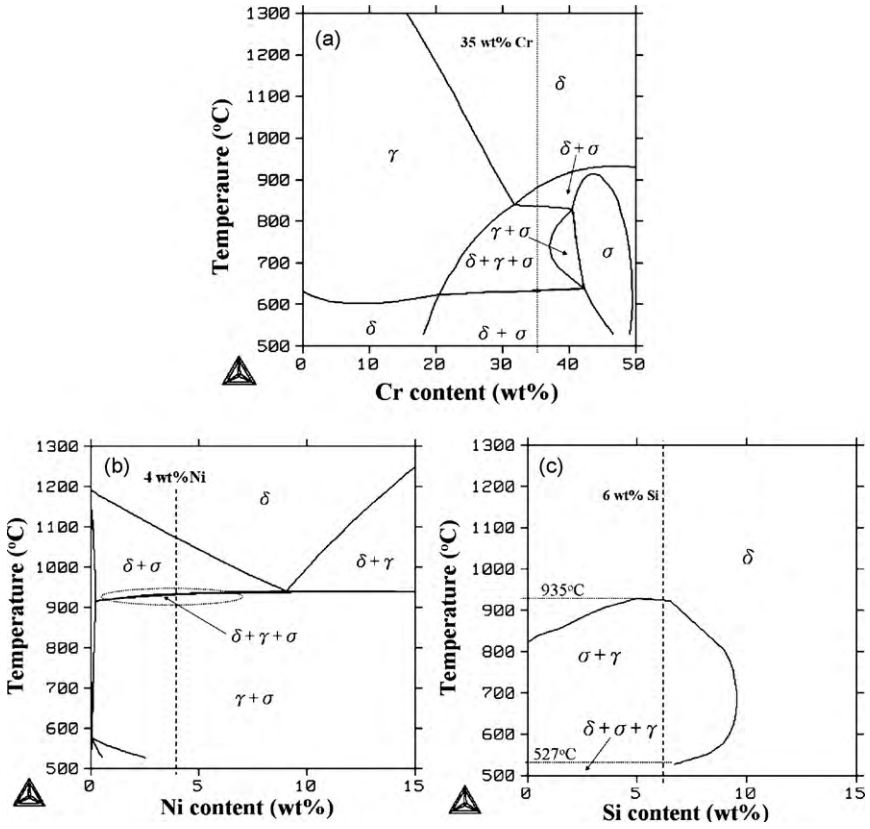

Fig. 7. Simulation of phase regions on the $\delta \rightarrow \sigma + \gamma_2$ phase transformation drawn from the FEDAT database of Thermo-Calc software with an increase of various elemental contents: (a) Cr content, (b) Ni content and (c) Si content.

Table 3
Diffusivities of the Cr and Ni in δ-ferrite and γ-austenite at various peak temperatures in accordance with the Vitek model.

Peak temperature (°C)	Diffusivity ($cm^2\ s^{-1}$)			
	D^{δ}_{Cr}	D^{γ}_{Ni}	D^{δ}_{Ni}	D^{γ}_{Cr}
678	1.31×10^{-13}	1.11×10^{-16}	1.00×10^{-13}	3.78×10^{-16}
861	1.74×10^{-11}	4.73×10^{-14}	1.34×10^{-11}	1.60×10^{-13}
893	3.52×10^{-11}	1.13×10^{-13}	2.71×10^{-11}	3.84×10^{-13}
934	8.14×10^{-11}	3.18×10^{-13}	6.26×10^{-11}	1.08×10^{-12}

D^{δ}_{Ni} : Diffusion coefficient of Ni in δ-ferrite, $cm^2\ s^{-1}$

D^{γ}_{Cr} : Diffusion coefficient of Cr in γ-austenite, $cm^2\ s^{-1}$

3.4. Thermo-Calc simulation of the $\delta \rightarrow \sigma$ phase transformation

The phase transformation of $\delta \rightarrow \sigma$ was examined using the steel database (FEDAT) of Thermo-Calc software (Version 2.2.1.1). The purpose of this simulation was to prove the previous experimental results and then observe the phase regions change of σ phase (56%Fe–35%Cr–4%Ni–6%Si) when in a temperature range of between 500 °C and 1300 °C.

The Cr content was regarded as a variable under a fixed composition (56%Fe, 4%Ni, and 6%Si). The effect of Cr content on phase region was discussed. When temperature ranged from 500 °C to 1300 °C, the changing order of the phase region was: $\delta+\sigma \rightarrow \delta+\gamma+\sigma \rightarrow \delta+\sigma \rightarrow \delta$, as shown in Fig. 7(a) and Eq. (5). However, the phase region was located in the $\delta+\gamma+\sigma$ area when temperature was 630–800 °C. This result showed the same tendency as seen in DSC thermal analysis. The phase transformation of $\delta \rightarrow \sigma$ could occur in the third pass fusion zone. The results of DSC analysis showed that it was located in the $\delta+\gamma+\sigma$ phase region when the peak temperatures were 861 °C, 893 °C, and 934 °C. The maximum simulated temperature was 830 °C due to the fact that Cr is not a main element used to enlarge the $\delta+\gamma+\sigma$ phase region under high temperatures:

$$\delta+\sigma \rightarrow \delta+\gamma+\sigma \rightarrow \delta+\sigma \rightarrow \delta \quad (5)$$

The Ni content was placed into a variable under a fixed composition (56% Fe, 35% Cr, and 6% Si) and the effects of the Ni content on phase region were discussed, as shown in Fig. 7(b) and Eq. (6). Compared with Eq. (5), the 2nd phase region was $\gamma+\sigma$ because Ni is a strong austenite stabilizer. The Ni content increased gradually and led to the γ phase precipitation so that the precipitated range of γ phase enlarged in the 1st phase region. Similarly, the single δ phase region existed at a temperature range between 1100 °C and 1300 °C:

$$\gamma+\sigma \rightarrow \delta+\gamma+\sigma \rightarrow \delta+\sigma \rightarrow \delta \quad (6)$$

Similarly, we regarded Si content as a variable under a fixed composition (56% Fe, 35% Cr, and 4% Ni) and discussed the effect of Si content on the phase region, as shown in Fig. 7(c) and Eq. (7). The first and second step phase region changed from $\delta+\gamma+\sigma$ (below 527 °C) into $\sigma+\gamma$. Hsieh et al. [22] have shown that Si can accelerate the phase transformation of $\delta \rightarrow \sigma$ so that no δ-ferrite can be found in the second step phase region.

Furthermore, Si can also enlarge the $\delta+\gamma$ phase region up to 935 °C. Drawing from DSC analysis result, this region was located at the peak temperatures (678 °C, 861 °C, 893 °C, and 934 °C) of $\delta \rightarrow \sigma$. It can be proven that the phase transformation of $\delta \rightarrow \sigma$ occurs at above peak temperatures. The δ-ferrite can exist at high temperatures ranging from 935 °C to 1300 °C:

$$\delta+\gamma+\sigma \rightarrow \sigma+\gamma \rightarrow \delta \quad (7)$$

3.5. Calculation of diffusion coefficient

The peak temperatures (678 °C, 861 °C, 893 °C, and 934 °C) taken from the DSC examination were substituted in Eqs. (8)–(23) allowing us to acquire diffusivities (D^{δ}_{Cr}, D^{γ}_{Ni}, D^{δ}_{Ni}, and D^{γ}_{Cr}). The transformation behavior of $\delta \rightarrow \sigma$ can be predicted efficiently by employing the diffusivity calculation from the Vitek model. A series of calculated results for diffusion coefficients are shown in Eqs. (8)–(23). Detailed values are listed in Table 3. Overall, it was found that diffusivities were increased when peak temperatures were increased from 678 °C to 934 °C. This can be attributed to thermal activated accelerated diffusion in the third pass fusion zone that occurred during multi-pass welding. The D^{δ}_{Cr} shows the highest value of all the diffusion coefficients. It had many vacancies to diffuse since both Cr and δ-ferrite are BCC structures when temperature ranges between 678 °C and 934 °C. Consequently, a higher diffusivity of Cr and Ni in δ-ferrite (D^{δ}_{Cr} and D^{δ}_{Ni}) and a lower diffusivity of Cr and Ni in γ-austenite will lead to the occurrence of $\delta \rightarrow \sigma$ phase transformation:

$$D^{\delta}_{Cr(678+273\,K)} = 2 \times \exp^{[-28{,}866/(678+273\,K)]} \quad (8)$$

$$D^{\delta}_{Cr(860.5+273\,K)} = 2 \times \exp^{[-28{,}866/(861+273\,K)]} \quad (9)$$

$$D^{\delta}_{Cr(893+273\,K)} = 2 \times \exp^{[-28{,}866/(893+273\,K)]} \quad (10)$$

$$D^{\delta}_{Cr(934+273\,K)} = 2 \times \exp^{[-28{,}866/(934+273\,K)]} \quad (11)$$

$$D^{\gamma}_{Ni(678+273\,K)} = 2.3 \times \exp^{[-35{,}722/(678+273\,K)]} \quad (12)$$

$$D^{\gamma}_{Ni(861+273\,K)} = 2.3 \times \exp^{[-35{,}722/(861+273\,K)]} \quad (13)$$

$$D^{\gamma}_{Ni(893+273\,K)} = 2.3 \times \exp^{[-35{,}722/(893+273\,K)]} \quad (14)$$

$$D^{\gamma}_{Ni(934+273\,K)} = 0.56 \times 2.3 \times \exp^{[-35{,}722/(934+273\,K)]} \quad (15)$$

$$D^{\delta}_{Ni(678+273\,K)} = \frac{2 \times \exp[-28{,}866/(678+273\,K)]}{1.3} \quad (16)$$

$$D^{\delta}_{Ni(861+273\,K)} = \frac{2 \times \exp[-28{,}866/(861+273\,K)]}{1.3} \quad (17)$$

$$D^{\delta}_{Ni(893+273\,K)} = \frac{2 \times \exp[-28{,}866/(893+273\,K)]}{1.3} \quad (18)$$

$$D^{\delta}_{Ni(934+273\,K)} = \frac{2 \times \exp[-28{,}866/(934+273\,K)]}{1.3} \quad (19)$$

$$D^{\gamma}_{Cr(678+273\,K)} = 3.4\{2.3 \times \exp[-35{,}722/(678+273\,K)]\} \quad (20)$$

$$D^{\gamma}_{Cr(861+273\,K)} = 3.4\{2.3 \times \exp[-35{,}722/(861+273\,K)]\} \quad (21)$$

$$D^{\gamma}_{Cr(893+273\,K)} = 3.4\{2.3 \times \exp[-35\,722/(893+273\,K)]\} \quad (22)$$

$$D^{\gamma}_{Cr(934+273\,K)} = 3.4\{2.3 \times \exp[-35{,}722/(934+273\,K)]\} \quad (23)$$

3.6. Precipitation mechanism of the σ phase

According to the results of the microstructure observation, diffusion calculation, and Thermo-Calc simulation, we constructed a schematic diagram to explain the above results. This is shown in

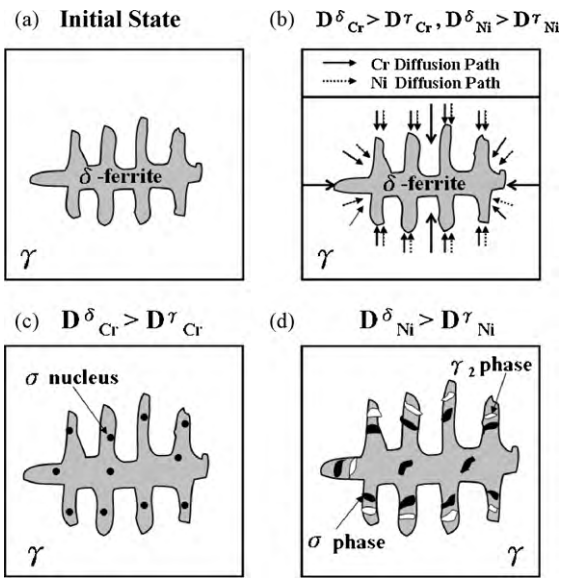

Fig. 8. Schematic diagram showing the mechanism of $\delta \rightarrow \sigma + \gamma_2$ eutectoid decomposition in the: (a) initial state, (b) diffusion of Cr and Ni in the δ-ferrite, (c) formation of σ nucleus and (d) precipitation of σ phase and secondary austenite (γ_2) in δ-particle.

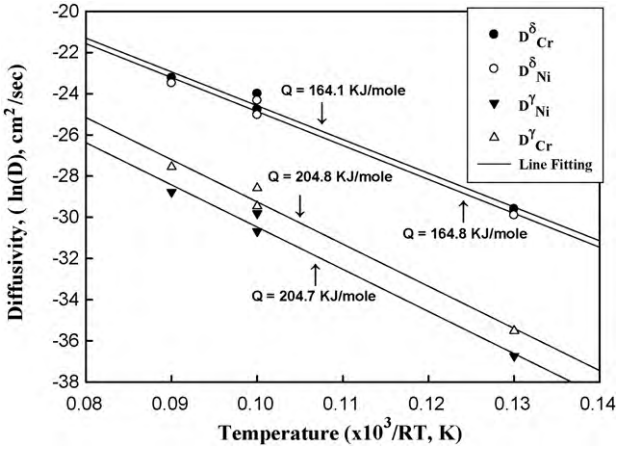

Fig. 9. Diffusion activation energies of the Cr and Ni in δ and γ phases at various peak temperatures.

Fig. 8(a)–(d). No diffusion of Cr and Ni occurred without welding and the δ-ferrite was stable at this stage, as shown in Fig. 8(a). The relationship between diffusion showed the $D^{\delta}_{Cr} > D^{\gamma}_{Cr}$ and $D^{\delta}_{Ni} > D^{\gamma}_{Ni}$, so that the Cr and Ni could be diffused into the δ-ferrite, as shown in Fig. 8(b). This means that Cr and Ni had higher diffusion rates in δ-ferrite than in the γ phase. Hence, the diffusion path of Cr and Ni was diffused toward to the δ-ferrite. When the diffusion relationship was $D^{\delta}_{Cr} > D^{\gamma}_{Cr}$,, the diffusion rate of Cr was higher in δ-ferrite than in the γ phase, as shown in Fig. 8(c). This generated a high Cr concentration region in δ-ferrite which became a beneficial site to form σ phases. In addition, Ni had a higher diffusion rate in δ-ferrite than it did in the γ phase when the diffusion relationship was $D^{\delta}_{Ni} > D^{\gamma}_{Ni}$,. Consequently, it was shown that higher Ni content can be reserved in δ-ferrite and that the secondary austenite formed in the δ-particles at the same time, as displayed in Fig. 8(d).

3.7. Calculation of diffusion activation energy

Both the diffusion coefficients (D^{δ}_{Cr}, D^{δ}_{Ni}, D^{γ}_{Cr}, and D^{δ}_{Ni}) and reciprocal peak temperatures ($(1/T_{P1})$, $(1/T_{P2})$, $(1/T_{P3})$, and $(1/T_{P4})$) can be used to calculate diffusion activation energies (Q^{δ}_{Cr}, Q^{δ}_{Ni}, Q^{γ}_{Cr}, and Q^{δ}_{Ni}). The diffusion activation energy can be used to estimate the ability of diffusion on the $\delta \rightarrow \sigma$ phase transformation of AISI 304 stainless steel at various peak temperatures in the third pass fusion zone. The calculated results of diffusion activation energies are shown in Fig. 9. It was observed that the diffusion activation energy of Cr in δ-ferrite was equal to that of Ni in δ-ferrite ($Q^{\delta}_{d\,Cr} \fallingdotseq Q^{\delta}_{d\,Ni}$). This means that the equivalent diffusion energy barrier for the diffusion of Cr and Ni in δ-ferrite is something to overcome in the $\delta \rightarrow \sigma$ phase transformation. Similar results were found for Cr and Ni diffusion in γ-austenite ($Q^{\gamma}_{d\,Cr} \fallingdotseq Q^{\gamma}_{d\,Ni}$). Therefore, the elemental diffusion of Cr and Ni was deemed efficient towards the δ-ferrite while it caused the precipitation of σ phase in δ-ferrite particles.

4. Conclusions

In this study, an examination method was investigated that used the Vitek diffusion equation and thermodynamic simulation for studying the phase transformation of $\delta \rightarrow \sigma$ in the fusion zones of dissimilar stainless steels that takes place during multi-pass welding process. Some significant results are summarized as follows:

(1) The phase transformation of $\delta \rightarrow \sigma$ occurs at peak temperatures of 678 °C, 861 °C, 893 °C, and 934 °C in the third pass fusion zone of dissimilar stainless steels from DSC analysis and Thermo-Calc simulation.
(2) The diffusivities of D^{δ}_{Cr} and D^{δ}_{Ni} had higher values than that of D^{γ}_{Cr} and D^{γ}_{Ni}, so that phase transformation of the $\delta \rightarrow \sigma$ can occur according to Vitek diffusion equation calculations.
(3) When the diffusion activation energies of Cr in δ-ferrite and γ-austenite are equal to that of Ni in δ-ferrite and γ-austenite ($Q^{\delta}_{d\,Cr} \fallingdotseq Q^{\delta}_{d\,Ni} \fallingdotseq 164$ kJ/mol) and $Q^{\gamma}_{d\,Cr} \fallingdotseq Q^{\gamma}_{d\,Ni} \fallingdotseq 204$ kJ/mol), phase transformation of the $\delta \rightarrow \sigma$ can occur.

Acknowledgement

The authors are obligated to thank the National Science Council and Ministry of Economic Affairs of the Taiwan, ROC for their financial support under the projects numbered 98-EC-17-A-08-S1-117, NSC98-2622-E-005-006-C2, and NSC98-2221-E-005-027.

References

[1] S. Missori, C. Koerber, Weld. J. 76 (1997) 125s–134s.
[2] P. Michael, S. Oliver, G. Thomas, Mater. Charact. 58 (2007) 65–71.
[3] R.F. Steigerwald, Corrosion 33 (1977) 338–343.
[4] H. Kiesheye, H. Brandis, Z. Metallkd. 67 (1976) 258–263.
[5] C.J. Park, M.K. Ahn, H.S. Kwon, Mater. Sci. Eng. A 418 (2006) 211–217.
[6] L. Karlsson, L. Ryen, S. Pak, Weld. J. 74 (1995) 28s–40s.
[7] T.H. Chen, K.L. Weng, J.R. Yang, Mater. Sci. Eng. A 338 (2002) 259–270.
[8] J.O. Nilsson, P. Kangas, T. Karlsson, A. Wilson, Metall. Trans. A 31 (2000) 35–45.
[9] L. Jianchun, W. Tuyan, R. Yves, Mater. Sci. Eng. A 174 (1994) 149–156.
[10] F.C. Hull, Weld. J. 52 (1973) 104s–113s.
[11] A. Atamert, J.E. King, J. Mater. Sci. Lett. 12 (1993) 1144–1147.
[12] M. Raghavan, R.R. Mueller, G.A. Vaughn, S. Floreen, Metall. Trans. A 15 (1984) 783–792.
[13] M. Subiel, B. Sepiol, Solid State Commun. 111 (1999) 613–618.
[14] A. Turnbull, P.E. Francis, M.P. Ryan, L.P. Orkney, A.J. Griffiths, B. Hawkins, Corrosion 58 (2002) 1039–1048.
[15] F. Liu, Y.H. Hwang, S.W. Nam, Mater. Sci. Eng. A 427 (2006) 35–41.
[16] S.H.C. Park, Y.S. Sato, Scripta Mater. 49 (2003) 1175–1180.
[17] D.Y. Lin, T.C. Chang, G.L. Liu, Scripta Mater. 49 (2003) 855–860.
[18] Y.S. Na, N.K. Park, R.C. Reed, Scripta Mater. 43 (2000) 585–590.
[19] H. Kokama, T. Kuwana, A. Yamamoto, Weld. J. 68 (1989) 92s–101s.
[20] C.C. Hsieh, D.Y. Lin, W. Wu, Mater. Sci. Eng. A 467 (2007) 181–189.
[21] J.M. Vitek, S.A. Vitek, S.A. David, Metall. Trans. A 26 (1995) 2007–2025.
[22] C.C. Hsieh, D.Y. Lin, T.C. Chang, Mater. Sci. Eng. A 475 (2008) 128–135.